CHAPTER 2.3 "Physical properties of magmas and their evolution during storage, transport, eruption and emplacement" – PART 1: Tectonics and plumbing systems

Authors:

Satoshi Okumura[1,*], Amelia A. Bain[2, 3], Magdalena Oryaëlle Chevrel[4], Jackie E. Kendrick[2], Edward W. Llewellin[5], Mattia Pistone[6], Alessandro Vona[7] and Alan Whittington[8]

1 Department of Earth Science, Graduate School of Science, Tohoku University, Miyagi, Japan

2 Department of Earth and Environmental Science, Ludwig-Maximilians-Universität (LMU), München, Germany

3 School of Geosciences, University of Edinburgh, Edinburgh, United Kingdom

4 Université Clermont Auvergne, CNRS, IRD, OPGC, Laboratoire Magmas et Volcans, Clermont-Ferrand, France

5 Department of Earth Sciences, Durham University, Durham, United Kingdom

6 Department of Geology, Franklin College of Arts and Sciences, The University of Georgia, Athens, USA

7 Dipartimento di Scienze, Roma Tre University, Roma, Italy

8 Department of Earth and Planetary Sciences, The University of Texas at San Antonio, San Antonio, USA

*Corresponding author: satoshi.okumura.d2@tohoku.ac.jp

This manuscript has been peer-reviewed and accepted for publication in The Encyclopedia of Volcanoes, 3rd Edition (Part 1: Tectonics and plumbing system).

ABSTRACT

Magma has played an important role in the Earth's evolution through volcanic and magmatic activity, including the formation of the crust and atmosphere. Magma storage, transport, eruption and emplacement can be quantitatively evaluated based on the understanding and knowledge of magma physical properties. In this chapter, the rheology, permeability and thermodynamic properties of magma are reviewed in the context of magma storage, transport and emplacement. Magma physical properties evolve due to changing temperature, pressure, crystallinity and other chemical, physical and thermal factors, which in turn, influence storage, transport and emplacement processes. The resulting feedbacks can strongly affect volcanic and magmatic activity.

KEYWORDS

Magma physical properties, silicate melt, thermal properties, rheology, viscosity, permeability, magma reservoir, magma ascent, lava flow

Introduction

Magma is generated and evolves in the Earth's interior and eventually erupts at the surface. These processes affect the evolution of the solid Earth, i.e., crust and mantle, from both physical and chemical perspectives [E1]. The surface environment in which humans live is also impacted by volcanic eruptions because those cause changes in the physicochemical conditions of the surface and atmosphere [E2]. These processes are controlled in part by the physical properties of magma. For instance, magma ascent to the surface is driven by buoyancy, resulting from decreasing magma density via gas bubble formation [E3]. The physical properties of magma also vary strongly with time due to evolving thermal gradients and kinetic limitations, so that disequilibrium can be important.

In this chapter, we focus on the physical and thermodynamic properties of magma and their evolution during storage, transport, and eruption. These properties not only influence these magmatic processes but also change in response to them, resulting in complex feedbacks (Fig. 1). To understand the evolution of the physical properties of magma during storage, transport, eruption and emplacement, first, we introduce theoretical and experimental understandings that depend on the interplay of pressure, temperature, crystallinity and other factors. Thermodynamic properties, rheology and permeability are the main focus of this section. The density and equation of state for silicate melts and mass diffusion are reviewed in the second edition of Encyclopedia of Volcanoes [E4]. We then discuss the changes in physical properties in storage and during transport, eruption and emplacement within reservoirs and conduits, and at the Earth's surface, along with their impact on volcanism and hazards.

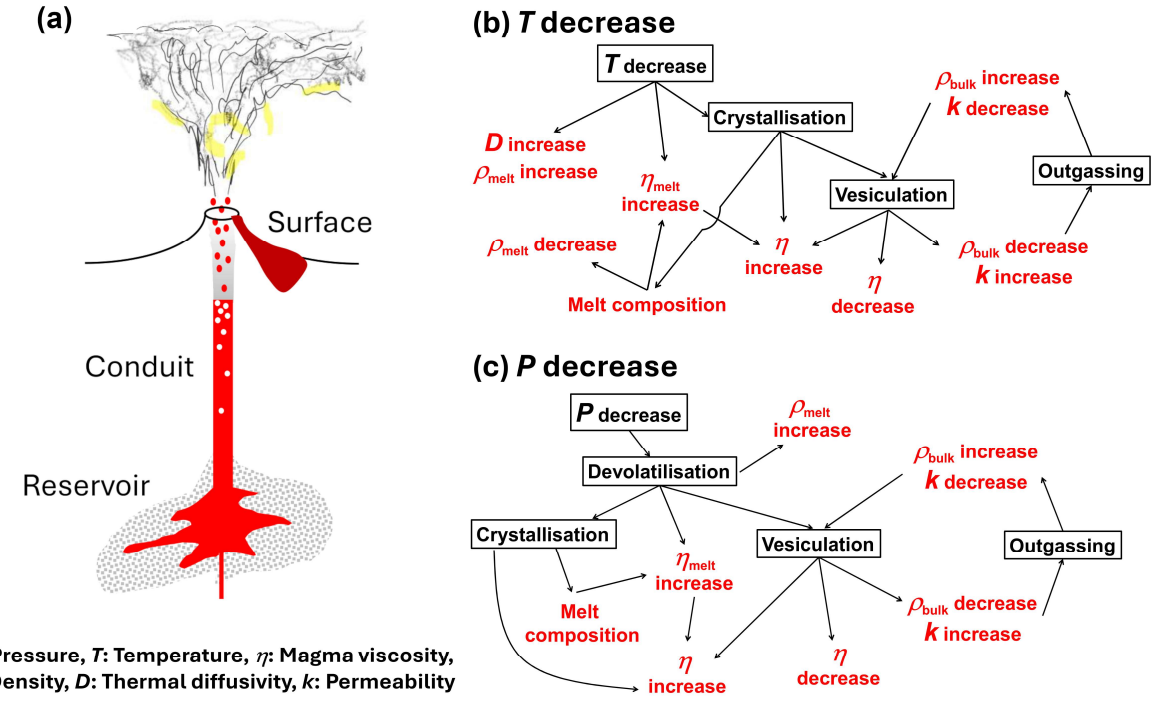

P: Pressure, T: Temperature, η: Magma viscosity, ρ: Density, D: Thermal diffusivity, k: Permeability

Figure 1. (a) Schematic of a shallow magmatic-volcanic system and eruption featuring lava flow emplacement. (b) and (c) illustrate magmatic processes (black), transport and thermodynamic properties (red) and their feedback during temperature (*T*) and pressure (*P*) changes. Parameters *T* and *P* decrease in the reservoir, within the conduit and at the surface, while *T* may increase by interaction with hotter magmas, crystallisation and shear heating during flow (see text).

Magma physical properties

Thermal properties of silicate melts and magmas

Heat content

The heat content of magmas (d*H*) includes both sensible heat, reflected in the heat capacity (C_p), and latent heat (ΔH), accompanying state changes such as melting and crystallisation (Fig. 2a). At constant pressure:

$$dH = \int C_P dT + \Delta H^{phase\ change}, \quad (1)$$

where *T* represents the temperature. Many detailed measurements have been made of the heat capacity of minerals. Stebbins et al. [1] provided composition-dependent models for the heat capacity of silicate glasses and melts. The heat capacity of rocks and minerals increases gradually with temperature, approaching a composition-dependent constant value. On reaching the solidus, the apparent heat capacity increases rapidly due to two factors. First, the heat capacity of liquids is higher than that of isochemical solids. Second, latent heat (enthalpy of fusion) must be supplied in addition to the sensible heat. In a differential scanning calorimeter, which measures a material's response to controlled temperature change, the rate at which melting occurs depends on factors such as heating rate and thermal contact between sample and pan, and liquidus temperatures are often overestimated, but latent heat of fusion can be measured accurately. The heat capacity of most silicate liquids is nearly independent of temperature, although the heat capacity of superheated liquids remains uncertain as few measurements exist.

Experimental data suggest that latent heat of fusion and of crystallisation typically varies from ~250 J g^{-1} for rhyolitic compositions to ~450 J g^{-1} for basaltic compositions. For temperature intervals between liquidus and solidus of typically 250–350˚C, this results in at least doubling the effective heat capacity (summing sensible and latent heat contributions) over the crystallisation interval (Fig. 2a). How latent heat is released as a function of temperature can be predicted from phase equilibria for slowly cooling systems, where latent heat release simply extends cooling timescales. The number of crystallising phases and rate of crystallisation (mol K^{-1}) usually increases as the temperature approaches the solidus, and so does the release of latent heat of crystallisation. Crystallisation in volcanic systems can occur under conditions of dramatic undercooling, due to rapid temperature reduction and/or volatile exsolution (devolatilisation), in which case rapid release of latent heat accompanying crystallisation can even lead to an increase of temperature during degassing-induced crystallisation.

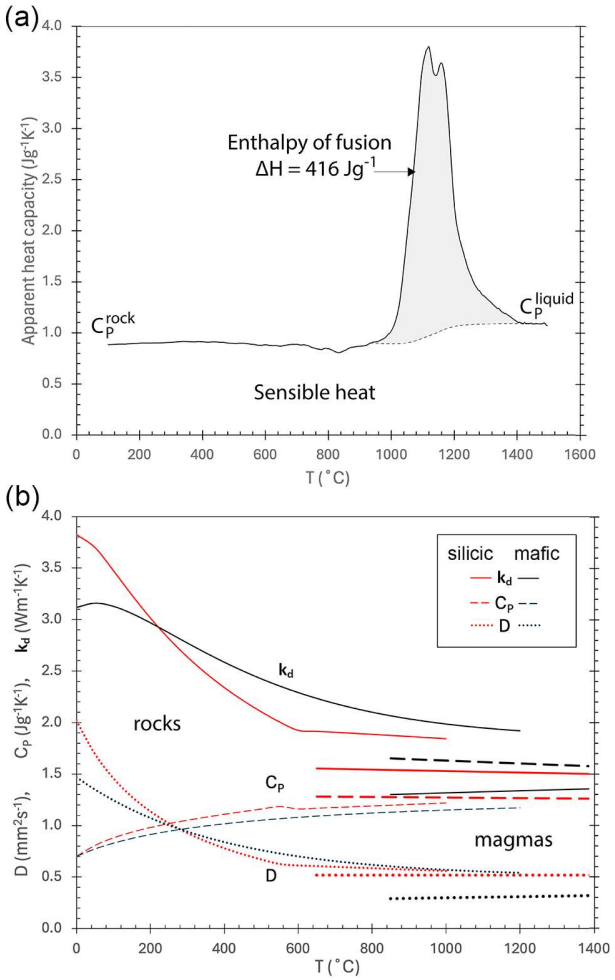

Figure 2. (a) Heat capacity of crystalline basalt from the 2018 Kilauea Lower East Rift Zone eruption, from Halverson et al. [14]. Grey shading indicates the enthalpy of fusion. Unshaded area below the heat capacity curve is sensible heat. (b) Thermal conductivity (k_d), heat capacity (C_p) and thermal diffusivity (D) as a function of temperature, for crystalline rocks (≤1000˚C for silicic and ≤1200˚C for mafic) and molten equivalents (bold lines; ≥650˚C for silicic and ≥ 850˚C for mafic). Granite from Whittington et al. [15], crystalline basalt from Merriman et al. [16], and rhyolitic and basaltic melt from Hofmeister et al. [3].

An additional phase change that is important in most volcanic systems is the exsolution of dissolved volatiles, primarily water, from silicate melt. Experimental data suggests that the enthalpy of exsolution of water from silicate melt is probably minor at magmatic temperatures, and will therefore not cause significant heating or cooling. However, water exsolution results in effective undercooling and can trigger crystallisation, which in turn will release latent heat. Resulting viscosity changes may be large in magnitude and complex, with devolatilisation and crystallisation both increasing the viscosity, while heating tends to decrease it. Such complex feedbacks are common and need to be incorporated into numerical models of conduit processes.

Heat transfer

Heat is transferred by three fundamental mechanisms: radiation, conduction and convection. Radiation is very important for heat loss from the surface of lava flows but radiative transfer within magma is often negligible as most melts are relatively opaque to thermal radiation, and the mean free path of phonons (lattice vibrations) is relatively short. Heat conduction occurs via the diffusion of phonons. Unlike chemical diffusion, thermal diffusion becomes slower at higher temperatures due to interference between phonons causing shorter mean free paths. Convection combines conduction and advection, and is potentially important in several different contexts in volcanic systems. For example, if convection occurs within magma chambers, it increases heat flux and cooling rates, as high temperatures are maintained at the chamber wall. Air convection on the upper surface of lava flows can be an important mechanism of heat loss, especially for forced convection due to externally driven wind.

Radiative heat loss from the surface of a lava flow is given by the Stefan-Boltzmann law:

$$Q_{rad} = \sigma_{SB} \varepsilon_s (T_s^4 - T_a^4), \quad (2)$$

where σ_{SB} is the Stefan-Boltzmann constant ($\sigma_{SB} = 5.67 \times 10^{-8}$ W m^{-2} K^{-4}), T_s is the temperature of the lava surface, T_a is the ambient temperature and ε_s is the thermal emissivity of the surface ($\varepsilon_s = 1$ for a black body). Although often assumed to be a constant value of approximately 0.95, ε_s is wavelength-dependent and consequently varies as a function of temperature, composition and crystallinity.

Time-dependent thermal diffusion is given by:

$$\frac{\partial T}{\partial t} = D \frac{\partial^2 T}{\partial x^2}, \quad (3)$$

where D is the thermal diffusivity (m^2 s^{-1}), which varies as a function of temperature, composition and crystallinity, often in the opposite direction to heat capacity (Fig. 2b).

Conductive heat flux is given by:

$$Q_{cond} = -k_d \frac{dT}{dx}, \quad (4)$$

where k_d is the thermal conductivity (W m^{-1} K^{-1}), obtained from $k_d = DC_P\rho$, where ρ is the density. For liquids, ρ can be calculated using the thermodynamic parameters in [E4], and for minerals it can be calculated from compilations of volume and thermal expansivity [2].

The temperature-dependence of D and k_d for liquids is small, while absolute values are typically lower for mafic liquids [3]. During crystallisation, both thermal diffusivity and conductivity increase, most strongly for mafic compositions. Crystallisation therefore both releases latent heat and allows it to be transported more efficiently. As crystallised lavas cool towards ambient temperature, their D and k_d values increase rapidly. Rapid cooling allows lava to suppress crystallisation and instead form glass, a disordered material that retains the atomic structure of the melt at the glass transition temperature.

Lavas that quench to glass also show increasing D and k_d on cooling, but much less strongly. The magnitude of changes in heat transfer properties with temperature and crystallinity is non-negligible, often being on the order of 50–100% for mafic lavas (Fig. 2b).

Convective heat loss from a surface is given by:

$$Q_{conv} = h_c(T_s - T_a), \quad (5)$$

where h_c is the heat transfer coefficient, which varies depending on the ambient medium, the temperature and whether convection is free or forced, for example by wind. For basaltic lava at ~500˚C and a wind speed of ~10 m s^{-1}, h_c is ~45–50 W m^{-2} K^{-1}, decreasing at lower temperatures and wind speeds.

Rheology

Crystal-free and bubble-free melts

Viscosity, representing the material's internal resistance to flow under stress, is a crucial physical property controlling magma transport within the Earth's interior and at the surface. Calculating the viscosity of ascending multiphase magmas undergoing chemical modification upon cooling and decompression requires the evaluation of the viscosities of both the liquid portion and bulk magma, the latter controlled by the modal proportion of minerals, gas bubbles and silicate melt that altogether capture the liquid, solid and gas state of matter in magmas.

Above the kinetic boundary of the glass transition temperature, melt is the liquid phase of the magma that behaves as a viscoelastic material as described by the Maxwell relationship: $\lambda = \eta/G_\infty$, where λ is the relaxation timescale, η is the shear viscosity, and G_∞ is the infinite-frequency elastic shear modulus of the melt. Under the application of stress, silicate melts span from liquid to glassy behaviour. The viscous-brittle transition of silicate melts is fundamental to nearly all hazardous volcanic phenomena, from explosive eruptions to endogenous dome failure and consequent volcanic blasts. The fluid and solid character of melts can be described by the Weissenberg number (Wi), which is defined by the relaxation timescale (λ) and deformation rate ($\dot{\gamma}$) ($Wi = (\eta \cdot \dot{\gamma}) / G_\infty$). At low Wi ($Wi < 10^{-3}$), silicate liquids are Newtonian. They take on an apparent non-Newtonian behaviour at $10^{-3} < Wi < 10^{-2}$ and fracture at $Wi > 10^{-2}$. The rheology of silicate melt is thus controlled by the competition between the deformation and the relaxation, which controls the level of elastic energy accumulated or dissipated within the silicate melt structure.

Silicate melt viscosity varies widely, spanning from 10^{-2} to 10^{14} Pa·s, primarily because of variations in temperature, melt composition and dissolved volatile contents, while other factors such as pressure may exert a secondary influence, with the viscosity of ascending melts typically increasing as the pressure decreases. Higher temperatures correlate with lower viscosities following a non-Arrhenian relationship that can be predicted with good approximation using multi-component empirical models applicable across a broad range of silicate melt compositions [4].

The compositional effect on viscosity is mainly controlled by the degree of polymerisation, which describes the level of arrangement of the silica tetrahedra (T) and non-bridging oxygens (NBO), whose ratio (NBO/T) defines how thick/viscous or thin/fluidal a silicate melt is. In general, silica-poor (mafic) magmas tend to have a high NBO/T (~0.50 < NBO/T < ~0.75 for anhydrous basalts), which defines their fluidal behaviour; whereas silica-rich (felsic) systems are characterised by low NBO/T (<~0.05 for anhydrous rhyolite), which favours high viscosity and potentially higher degree of brittle behaviour at equivalent deformational conditions when compared to mafic melts. The viscosity offset between mafic and felsic melts is also exacerbated by their different eruption temperature: mafic melts erupt at hotter temperatures than felsic compositions.

A chemical component that largely controls the viscosity of silicate melts is water: the higher the water concentration in the melt, the lower the viscosity. Water solubility in silicate melts is controlled by melt composition, crystallisation upon cooling and, above all, by pressure. Water exsolution upon decompression during magma ascent can favour an increase of melt viscosity by many orders of magnitude, especially as water concentration drops below 1 wt.%.

The effect of temperature, chemical compositions and water contents on melt viscosity is summarised in Figs. 5.4 and 5.5 of the second edition of Encyclopedia of Volcanoes [E4].

Two-phase magma suspensions

Upon cooling and/or devolatilisation, silicate melts can experience crystallisation and become crystal-bearing suspensions. Such a process is initiated with the formation of nanocrystals or nanolites (i.e., crystals of nanometre size) and can favour an increase in viscosity, as a consequence of the modification of the melt composition and the onset of particle–particle interactions. When minerals grow to sizes relevant to microlites and phenocrysts, the modal proportion of minerals (ϕ) dictates the non-linear variation of magma viscosity and favours non-Newtonian behaviour. At this point, magma viscosity becomes a complex function of stress, strain rate and strain.

Over the last four decades, numerous experimental and computational studies have been conducted to quantify the rheology of crystal-bearing magmas. As the modal proportion of minerals increases, magma suspension viscosity (commonly expressed as relative viscosity, the dimensionless ratio of multiphase magma viscosity over melt viscosity) exhibits a sigmoidal increase, reflecting different flow regimes from dilute suspensions with non-interacting particles to concentrated and hyper-concentrated magma suspensions congested by solid-solid interactions (Fig. 3).

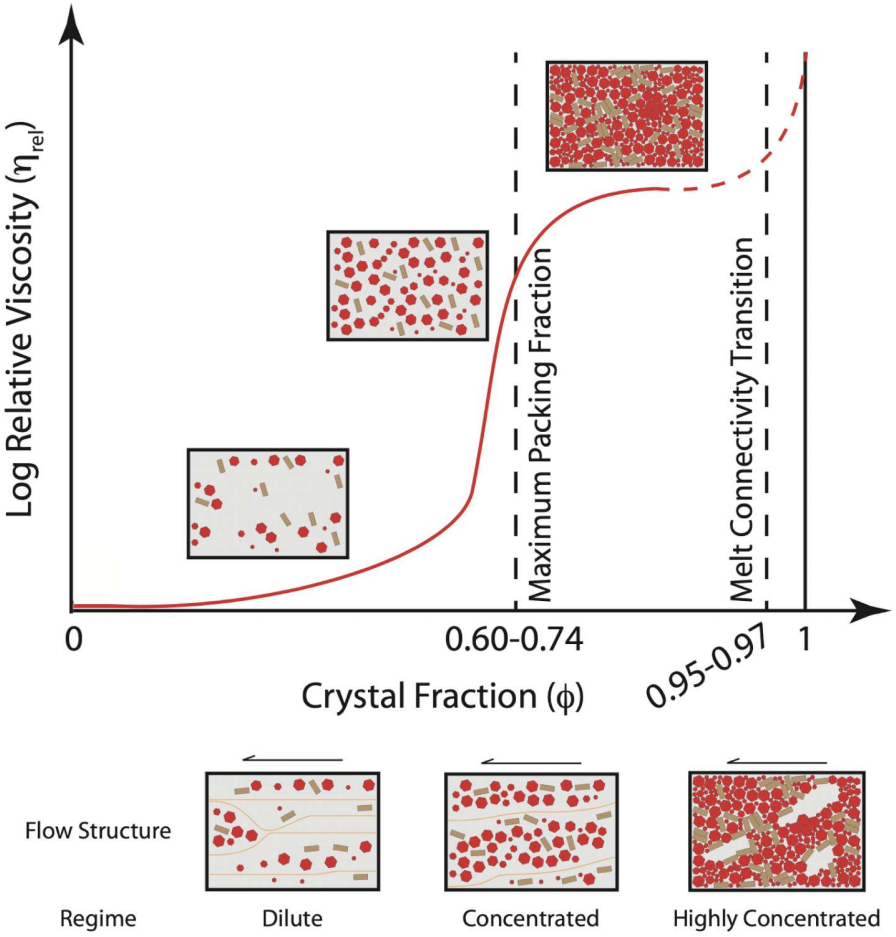

Figure 3. Non-linear increase in magma viscosity with increasing crystallinity in the relative viscosity-crystal volume fraction space for crystal-bearing systems devoid of gas bubbles. The variation of relative viscosity and rheological regimes as a function of crystal fraction highlights three rheological regimes: i) a Newtonian stage for dilute suspensions below a critical volume fraction of crystals for their mutual interactions, ii) non-Newtonian behaviour of concentrated suspensions approaching the maximum crystal volume fraction, triggering a sudden increase in magma viscosity, and iii) non-Newtonian to Mohr-Coulomb (brittle) behaviour of hyperconcentrated suspensions approaching the melt connectivity transition beyond which magma viscosity cannot be estimated.

The rheological transition from dilute to concentrated suspensions is represented by the maximum packing fraction of particles (ϕ_m) that defines whether the deformational mechanisms are primarily controlled by the melt phase or the suspended minerals in the magma. The maximum packing fraction is described as:

$$\phi_m = \phi_{m1} \exp\left[-\frac{(\log_{10} r_c)^2}{2b^2}\right], \quad (6)$$

where r_c is the mean aspect ratio, ϕ_{m1} is the maximum packing fraction for monodisperse particles with r_c = 1 and b is a fitting parameter (ϕ_{m1} = 0.55 and b = 1 [5]). When $\phi/\phi_m < 0.5$, the suspension can be approximated to a Newtonian fluid, whereas, at higher crystal contents, non-Newtonian behaviours such as shear thinning (decrease of magma viscosity with increasing strain rate) and apparent yield stress development (at $\phi/\phi_m > 0.8$) occur (Fig. 3). Both the maximum packing fraction and the overall non-linear viscosity increase with increasing crystallinity are controlled by the mineral shape and size distributions, as well as mineral orientation within the liquid suspension.

Specifically, ϕ_m decreases when the aspect ratio of particles deviates from unity. As a result, at equivalent crystallinity, a magmatic suspension dominated by elongate particles (with aspect ratio >1) favours higher viscosity compared to suspensions dominated by equant particles. However, under high shear rates, anisometric particles can align to the flow direction inducing a reduction in magma viscosity. Also, crystal size and size polydispersity exert a strong control on ϕ_m and the relative viscosity increases. Additionally, suspensions with bimodal (e.g., phenocrysts and microlites) or highly dispersed particle size distributions achieve more efficient crystal packing, reducing the interaction between crystals, shifting the ϕ_m to higher crystal contents and thus decreasing suspension viscosity for a given crystallinity.

In the last decades, several efforts have been made to parametrise the effect of crystals on magma viscosity. Two strategies have been applied to the model: a) the dilute regime ($\phi < \phi_m$) [5] and b) the rheological behaviour across the entire spectrum of suspended solid fractions ($0 < \phi < 1$) [6]. The functional formulations of semi-empirical models used for dilute suspensions produce an asymptotic increase in viscosity as the particle concentration approaches $\phi = \phi_m$, rendering them inapplicable at higher crystal fractions. Crystal-bearing magma rheology is described as a Herschel-Bulkley fluid, whose flow behaviour is defined by:

$$\tau = \tau_0 + K\dot{\gamma}^n, \tag{7}$$

where τ is the shear stress, τ_0 is the yield stress, $\dot{\gamma}$ is the strain rate, n is the flow index ranging from 1 for Newtonian fluids to $n < 1$ for shear thinning fluids, and K is the flow consistency corresponding to shear viscosity ($\eta = \tau/\dot{\gamma}$) when n =1 and/or $\dot{\gamma} = 1$.

When $\phi/\phi_m < 0.5$, the suspension behaves as a Newtonian fluid ($\tau_0 = 0$ and $n = 1$). In this case, the effect of crystals on magma viscosity is a simple function of crystal content and shape, and the relative viscosity (η_r) is described by Maron and Pierce [7] as:

$$\eta_r = \frac{\eta}{\eta_l} = \left(1 - \frac{\phi}{\phi_m}\right)^{-2}, \tag{8}$$

where η_l represents the viscosity of a particle-free fluid.

When $0.5 < \phi/\phi_m < 0.8$, magmas display non-Newtonian shear thinning behaviour ($n < 1$) and the absence of a yield stress ($\tau_0 = 0$). In this case, Eq. 7 reduces to that of a power law fluid and the relative viscosity ($\eta_r = \eta/\eta_l$) becomes:

$$\eta_r = K_r \dot{\gamma}^{n-1}, \tag{9}$$

where $K_r = K/\eta_l$ is the relative consistency, that in analogy with Eq. 8, is modelled as:

$$K_r = \frac{K}{\eta_l} = \left(1 - \frac{\phi}{\phi_m}\right)^{-2}, \tag{10}$$

whereas the flow index is empirically given by [5]:

$$n = 1 - 0.2R\left(\frac{\phi}{\phi_m}\right)^4. \tag{11}$$

Finally, for $\phi/\phi_m > 0.8$, the suspension develops appreciable yield stress ($\tau_0 \neq 0$) and the flow is described by the Herschel-Bulkley model (Eq. 7). Although several studies observed a rapid increase in yield stress with increasing ϕ/ϕ_m, a simple relation between ϕ_m, R and τ_0 is not available.

In the full spectrum of crystallinity, a semi-empirical parameterisation of relative viscosity first proposed by Costa [6], revised by Frontoni et al. [8], is based on an equation dependent on four parameters that describe the variation of the viscosity of particle-bearing mixtures as a function of the crystal volume fraction:

$$\eta_r = \frac{1+\varphi^\delta}{[1-F(\varphi,\varepsilon,\gamma)]^{B\phi^*}}, \tag{12}$$

where

$$F = (1-\xi)\mathrm{erf}\left[\frac{\sqrt{\pi}}{2(1-\xi)}\varphi(1+\varphi^\gamma)\right], \tag{13}$$

with B the Einstein coefficient ($B = 2.5$), $\varphi = \phi/\phi^*$, and ϕ^*, ξ, γ and δ being the empirical parameters that depend on the strain rate and particle shape (Fig. 4).

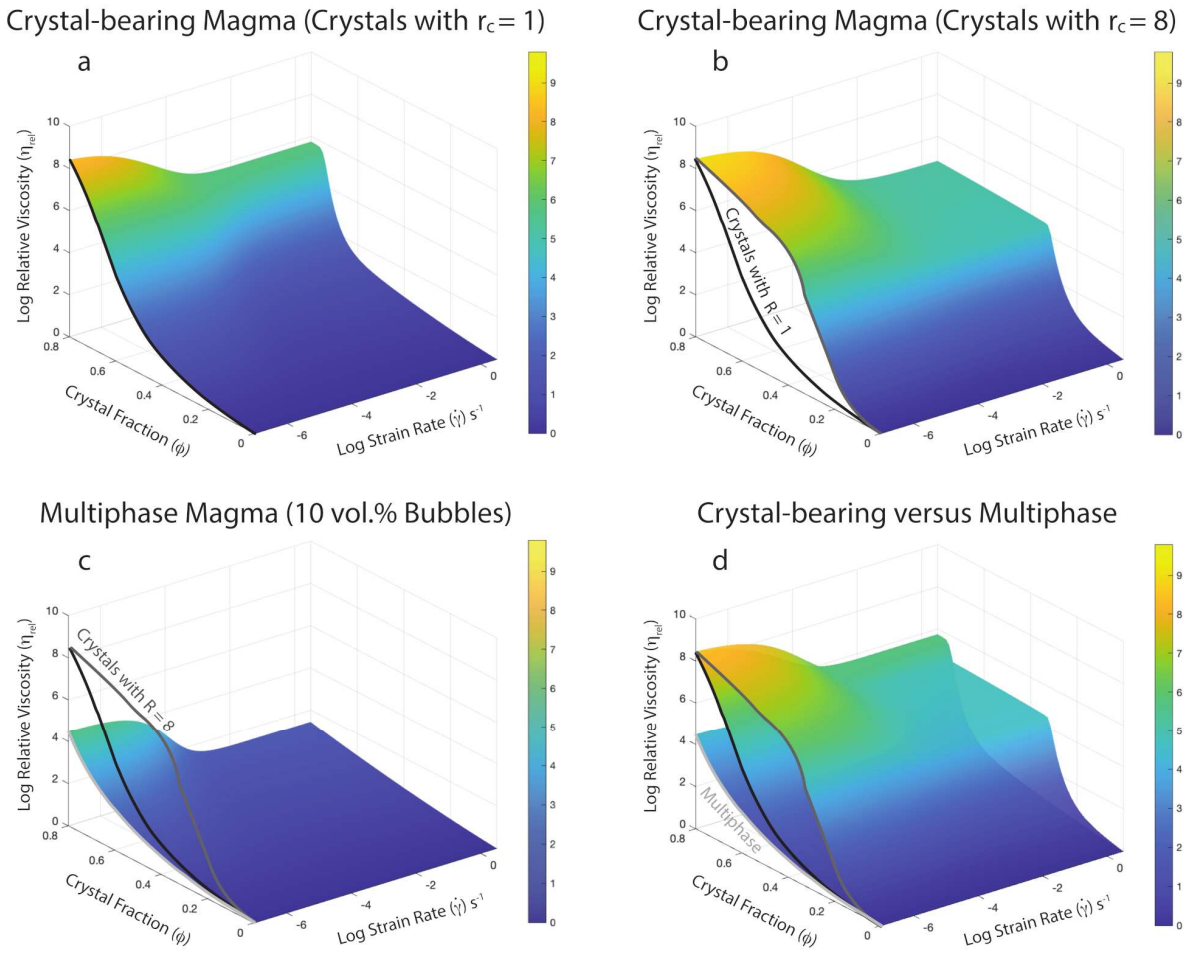

Figure 4. Three-dimensional plots showing the different rheological behaviours in the relative viscosity, strain rate and crystal volume fraction space for crystal-bearing magmas with (a) equant crystals (aspect ratio r_c = 1), (b) elongate crystals (r_c = 8), (c) equant crystals (r_c = 1) and 10 vol.% gas bubbles and (d) their direct comparison highlighting the rheology of multiphase magmas. These plots are quantified based on the models of Frontoni et al. [8] for crystal-bearing systems and Pistone et al. [10] for multiphase magmas.

The rheology of crystal-free bubble-bearing magmas depends on the bubble relaxation timescale and the steadiness of flow [5]. Melt viscosity (η_l), bubble radius (r) and the interfacial tension between the fluid in bubbles and the melt (σ) dictate the bubble relaxation time ($\lambda_b = (\eta_l \cdot r)/\sigma$). For steady flows (i.e., shear is constant or changing slowly with respect to the relaxation time), the capillary number ($Ca = \lambda_b \cdot \dot{\gamma}$) modulates the rheological response of the bubble-bearing suspension. When λ_b is less than the deformation time (related to the strain rate, $\dot{\gamma}$) (i.e., $Ca \ll 1$), interfacial forces act to reduce the surface energy and return bubbles to spherical shapes. At this condition, spherical bubbles act as rigid objects like minerals, hindering viscous flow of the melt. In contrast, when λ_b is greater than the deformation

time (i.e., *Ca* $\gg$ 1), the viscous forces dominate and inviscid bubbles deform during flow, reducing magma viscosity.

To define the degree of unsteadiness of a suspension, Llewellin et al. [9] propose the dynamic capillary number (*Cd*) as a ratio between the bubble relaxation time and the characteristic timescale that compares the rate of change of strain rate ($\ddot{\gamma}$) with the strain rate itself ($\dot{\gamma}$): *Cd* =$\lambda(\ddot{\gamma}/\dot{\gamma})$. At *Cd* $\ll$ 1, the bubbles are able to respond continuously to the changes in shear environment, the flow can be considered steady and the viscosity regime is defined by *Ca*. Conversely, at *Cd* $\gg$ 1, the flow is unsteady and *Ca* is undefined, since the shear environment is changing too rapidly for the bubbles to relax. Consequently, bubbles' elastic response to shear is suppressed and, thus, their viscous response leads to a reduction in magma viscosity. During deformation, bubble shape tends to become oblate and prolate in unsteady and steady flow conditions, respectively.

To date, the most widely applicable rheological model for crystal-free bubble-bearing suspensions combines *Ca* and *Cd* into a single parameter termed the capillarity parameter ($Cx = \sqrt{Ca^2 + Cd^2}$) and provides three equations for the relative viscosity of the bubble-bearing suspension in different *Cx* regimes [5]:

$$\eta_r = \begin{cases} \eta_{r,0}, & Cx < 0.1, \\ \eta_{r,\infty} + \frac{\eta_{r,0} - \eta_{r,\infty}}{1 + Cx^m}, & 0.1 < Cx < 10, \\ \eta_{r,\infty}, & Cx > 10, \end{cases} \tag{14}$$

where *m* = 2 and

$$\eta_{r,0} = (1 - \phi_b)^{-1}$$

$$\eta_{r,\infty} = (1 - \phi_b)^{\frac{5}{3}},$$

where ϕ_b represents the volume fraction of gas bubbles.

Three-phase magma suspensions

To date, relatively few studies have explored the rheology of multiphase magmas containing crystals, gas bubbles and melt in different modal proportions. These studies have demonstrated that three-phase magmas show complex rheological behaviour due to mutual interactions between crystals, gas bubbles and melt in suspension, leading to strain-rate dependence (shear thinning and thickening, indicating decrease and increase in magma viscosity with increasing strain rates, respectively) and strain dependence (strain weakening and hardening, which consist of viscosity decrease and increase with strain, respectively).

Multiphase suspensions are characterised by local spatial arrangements of crystals, gas bubbles and melt during deformation, depending on the respective volume fractions, sizes, interactions of phases and stress/strain rate partitioning within the textural domain of magmas. Textural arrangements of crystals and/or bubbles (e.g., crystal alignment, bubble elongation, etc.) are highly sensitive to strain rate-dependent processes. At high crystallinity, bubbles may help to accommodate shear localisation. In some regimes, at low crystallinity, bubbles may be able to connect during deformation, enhancing gas permeability and promoting outgassing. Even relatively small bubble volume fractions may significantly reduce crystal-bearing magma viscosity [10] (Fig. 4).

Available three-phase rheology models are mainly based on the combination of two-phase constitutive equations employing the effective medium approach [11]. The effective medium approach consists of estimating first the relative effect of one phase (the smallest, either crystals or bubbles) within the melt. Then this mixture is designated as the effective medium and will be used to estimate the influence of the other phase relative to it. The effective medium approach is very convenient because any combinations of two-phase models can be applied. However, this approach neglects the dynamics of mutual interactions between crystals and gas bubbles. This approach is used in the case study box and the supplementary exercises.

Another approach used to quantify the rheology of multiphase magmas consists of applying a modified Dorn-type Arrhenius equation [12], which includes the dependence of the flow parameters on the volumetric fractions of crystals, bubbles and melt, and their mutual interactions during magma deformation: $\dot{\gamma} = A \cdot \tau_u^n \exp(-Q/RT)$, where A is the pre-exponential term ($MPa^{-n}\ s^{-1}$), τ_u is the applied stress (MPa), n is the stress exponent, Q is the activation energy ($J\ mol^{-1}$), T is the absolute temperature (K), and R is the gas constant (8.314 $J\ K^{-1}\ mol^{-1}$). Each of these factors depends on χ, which is the fraction of weak phases. Depending on the relative proportions of melt, gas bubbles and crystals, the χ parameter can be: 1) the sum of melt and gas bubble fractions ($\chi = \mu + \phi_b$), when gas bubbles are deformable ($Ca > 1$) and the magma is crystal-rich ($\phi > 0.44$); 2) the gas bubble fraction only ($\chi = \phi_b$), when gas bubbles embedded in high-viscosity melt are deformable ($Ca > 1$) and the magma is crystal-free or -poor ($\phi < 0.44$); 3a) the melt fraction only ($\chi = \mu$), when gas bubbles do not deform and effectively behave like solid particles ($Ca < 1$), thereby the bubble volume fraction contributes to the crystal volume fraction; 3b) the melt fraction only ($\chi = \mu$), when gas bubbles are entirely removed from the magma by shear-induced outgassing ($\phi_b = 0$). The proposed empirical approach allows the mapping of the strain rate and viscosity partitioning within the magmas, and the quantification of microscopic deformation mechanisms in the microstructural domains of multiphase magmas by retrieving information on the flow behaviour of magmas from analyses of natural volcanic products. Modelling multi-phase magma rheology is an active research topic and a likely key area of focus in the next decade.

In the case study box, we estimate the one-, two- and three-phase viscosity of magma erupted during the 1980 activity of Mount St. Helens. Further details of these calculations are also provided in the supplementary exercises.

Permeability

Permeability describes how easily a fluid can flow through porous solid (or effectively solid) media. Two main permeable flow scenarios are of relevance to the physical volcanology of magma transport

and eruption: 1) permeability of foamy, fractured or granular magma to gas; 2) permeability of a mushy reservoir to melt. In all cases, permeable flow requires that the fluid phase is connected across the domain and that there is a pressure gradient to drive flow. The relationship between permeability, pressure and flow is commonly described by Darcy's law in one dimension:

$$q = -\frac{k}{\mu_f}\frac{\Delta P}{L}, \tag{15}$$

where q (m s^{-1}) is the fluid flux per unit area, k (m^2) is the Darcy permeability, $\Delta P/L$ (Pa m^{-1}) is the driving pressure gradient in the direction of flow and μ_f (Pa·s) is the fluid viscosity. Permeability may be anisotropic, particularly in the case of sheared or fractured magma; in such cases, a tensorial form of Darcy's law should be used. Darcy's law assumes creeping fluid flow; for scenarios in which inertia is important (e.g., for rapid gas flow), the Forchheimer equation should be used. In that case, the relationship between permeability, pressure and flow should be described by the following Forchheimer equation:

$$\frac{\Delta P}{L} = -\frac{\mu_f}{k}q - \frac{\rho_f}{k_F}q^2, \tag{16}$$

where k_F (m) is the inertial permeability and ρ_f (kg m^{-3}) is the fluid density.

The Darcy permeability depends strongly on the porosity of the solid medium and on the size and geometry of the pores. In general, the dependence must be determined by laboratory or numerical experiment, which typically yields a relationship of the general form:

$$k = l^2 f(\alpha), \tag{17}$$

where l (m) is a characteristic pore length-scale, α is the porosity and $f(\alpha)$ depends on the geometry, often taking the form of a power law. When considering the flow of gas in vesiculated magmas, α is the same as ϕ_b.

The gas permeability of magmas is particularly critical for one phenomenon: outgassing of magmatic volatiles. It is critical because it mitigates eruption explosivity. Two main mechanisms for permeable outgassing have been proposed: the 'permeable foam' model in which gas escapes through connected bubbles (Table 1 A,B); and the 'fracture/tuffisite' model in which gas escapes through fractures in the magma and adjacent wall rock, which may be ash-filled (Table 1 C,D). Two examples appropriate to these two models (A, B and C, D for the permeable foam and fracture/tuffisite models, respectively) are given in Table 2. The gas permeability of magmas depends strongly on their porosity (fraction of bubbles), and the interconnection and pore aperture size of the connected bubble networks.

The evolution of gas permeability during vesiculation and outgassing is hysteretic: permeable flow onsets at ϕ_b = 0.3–0.7 during vesiculation but persists down to much lower porosity during densification through outgassing. Measured values for pumice and dome rocks typically fall in the range of $10^{-16} \leq k \leq 10^{-10}$ m^2. The permeability of fractured rock is complex, depending on crack width, extent and connectivity. Progressive welding of ashy crack infill decreases the transport efficiency of cracks over time.

Permeability is also relevant for the extraction of melt from crystal-rich magmatic mushes. The connected porosity comprises interstitial melt around packed crystals, which is a similar geometry to the well-studied problem of fluid flow in sediments; hence, variants of the Kozeny–Carman equation are often used. For a packed particle system, the following form is obtained:

$$k = \frac{d^2}{180}\frac{\alpha^3}{(1-\alpha)^2}, \tag{18}$$

where *d* [m] is the mean equivalent spherical diameter of the particles. Typical values for magma reservoirs fall in the range of $10^{-10} \leq k \leq 10^{-5}$ m^2. Permeability decreases with compaction or crystallisation and increases with dilation or melting induced by magma recharge.

Table 1. Permeability parameters appropriate to different scenarios; refer to Equation 17.

Scenario		Length-scale	Porosity function	Reference
Permeable foam	(A)	$l = 2.88 \times 10^{-3} r$	$f(\phi_b) = (\phi_b - \phi_c)^{2.1}$	Blower [17]
		r (m) is mean pore radius, $\phi_c \approx 0.3$ is critical porosity for onset of permeability ($f(\phi_b) = 0$ for $\phi_b < \phi_c$). Derived from analysis of conductance of networks of pore–pore apertures.		
	(B)	$l = c_1$	$f(\phi_b) = (\phi_b - \phi_c)^n$	Mueller et al. [18]
		Values determined by experiment on natural pumices and dome lavas. Effusive products (fractures, elongate vesicles): $c_1 \approx 3.2 \times 10^{-6}$; $\phi_c = 0$; $3 \lesssim n \lesssim 3.8$ Explosive products (sub-spherical vesicles): $c_1 \approx 3.2 \times 10^{-5}$; $\phi_c = 0.3$; $n = 2$		
Fracture/Tuffisites	(C)	$l = \frac{wH}{\sqrt{12}}$	$f(\alpha) = \alpha$	Zimmerman and Bodvarsson [19]
		w [m] is fracture width, H is a dimensionless parameter that describes fracture wall roughness with $H = 1$ for a smooth fracture and $H < 1$ for rough walls.		
	(D)	$l = \frac{\sqrt{2[1-(\alpha-\alpha_c)]}}{3(1-\alpha)\ln(1-\alpha)}\frac{\langle a^3\rangle}{\langle a^2\rangle}$	$f(\alpha) = (\alpha - \alpha_c)^{4.4}$	Wadsworth et al. [20]
		Derived for welding ash packs (e.g. in tuffisites); l derives from percolation theory, $\langle a^i\rangle$ is the i^{th} moment of the pore size distribution, $\alpha_c = 0.03$		

Evolution of magma physical properties during storage, transport, eruption and emplacement

Evolution in the crustal reservoir

In the crustal reservoir, the magma is cooled through the interaction with crustal rocks. The cooling processes are contributed by thermal diffusion, convection and assimilation. At the initial stage of the cooling, the magma contains only a small fraction of crystals and displays liquid-like behaviour, resulting in active convection and assimilation, and thus high cooling rates. With a decrease in temperature

resulting in increasing crystallinity, magma viscosity increases, resulting in a decrease in the convection rate (Fig. 1b). Thermal diffusion gradually becomes a dominant process for cooling. These cooling processes modulate the evolution of magma's physical properties in the reservoir. The cooling processes are affected by the physical properties of magma and hence magma processes and physical properties have feedback effects on each other (Fig. 1b).

Magma crystallisation through cooling causes changes in melt composition (Fig. 1b). All the changes in temperature, melt composition and crystallinity strongly influence the viscosity and density of the magma (Fig. 1b). In particular, the viscosity increases with temperature reduction, SiO_2 enrichment of the melt, and crystallinity increase. Crystallisation can also cause volatile exsolution due to the enrichment of volatiles in the residual melt [E3], which induces an increase in the buoyancy of magma through the formation of gas bubbles with low density (Fig. 1b). As a result, the crystallisation of magma in the reservoir results in an increase in viscosity and also a decrease in density. The density reduction can drive the ascent of magma, while the viscosity increase hinders magma ascent [E5]. Gas bubbles also tend to lubricate crystal-rich magmas. These complicated feedbacks ultimately control whether magma can erupt or not.

Reheating by magma injection can result in a decrease in magma viscosity through the increase in temperature and crystal dissolution. This heating may also induce a density reduction via the change in volatile solubility and vesiculation [E3]. There are many petrological signatures of heating, such as dissolution textures and elemental distributions in phenocrysts, as well as evidence of magma mixing, such as non-equilibrium phenocryst assemblages and chemical compositions that show a mixing trend, but the actual process of heating remains controversial. For instance, injected magmas with high temperatures but relatively mafic compositions commonly have higher densities than that in the reservoir. The density contrast between two magmas hinders efficient mixing and instead tends to yield layered zones at the base of reservoirs. In this case, extensive mixing appears to be difficult, and an unknown physical mechanism may contribute to the heating and mixing processes. All these processes are related to each other, controlling the initiation of magma ascent and eruption, and inducing complicated eruptive behaviour, although the injection of magma into the reservoir is often and simply thought to be a trigger mechanism for eruption.

Evolution during ascent and eruption

In this section, we detail the current understanding of how magma's physical properties evolve during the ascent to the surface, and how this may influence eruption style. Conditions of magma ascent are highly variable as well as those of magma storage. These conditions remain relatively poorly understood as a result of the dynamic evolution of the crystal cargo, volatile solubility and temperature during ascent. Perturbations in pressure (related to loading/unloading or magma/volatile injection) or temperature (related to the injection of new magma) may disrupt the state of stored magma and trigger devolatilisation and vesiculation that drives ascent toward the surface via the reduction of magma density.

During ascent, all magmas experience decompression, devolatilisation, crystallisation and temperature changes, to differing extents (Fig. 1c). Typically, magmas contain up to a few weight percent of dissolved volatiles, in particular H, C, S and halogens Cl and F. Volatile solubility is dictated by pressure, temperature, magma composition and oxidation state. Magma decompression triggers volatile exsolution,

driving bubble formation, and increasing the buoyancy favouring magma ascent. Importantly, this depends on the composition of the magma and tectonic setting, which influence the concentration and ratios of volatiles in the magma [E3].

Dissolved volatiles must migrate through the melt to exsolve, thus the timescales of devolatilisation of different volatile species vary according to their diffusion rate, dynamically shifting the ratios of different gas species in the bubbles during ascent. For a given melt composition, lower dissolved volatile contents result in higher melt densities and viscosities. Bubble formation requires a degree of super-saturation as the nucleation of bubbles consumes energy. In the case of a fully molten system, the nucleation is also controlled by viscosity, surface tension and volatile element diffusivity. Hence, bubble number density (BND) may be quantitatively linked to decompression rate for melts of specific composition, with higher rates of decompression leading to higher BND. When crystals are present, bubble nucleation is heterogeneous as bubbles preferentially nucleate on existing solid surfaces (which reduces the energy required). The abundance and mineralogy of crystal cargo will dictate whether BND can be correlated to decompression rate.

During ascent, multiple interacting processes can trigger magma vesiculation (Fig. 1c), modifying and overprinting the bubble networks created at depth. For example: decompression allows bubbles to expand and coalesce, and drives further devolatilisation; crystallisation provides nucleation sites for new bubbles and restricts the space available for bubble growth, enhancing coalescence; bubble coalescence promotes outgassing and magma densification (Fig. 1c). Likewise, devolatilisation shifts mineral stability, which can trigger crystallisation. Episodic ascent with periods of stalling may allow time for equilibration of volatile contents, growth of microlites, and development of permeability by bubble coalescence, which may allow passive outgassing. In contrast, steady ascent rates may favour maintained homogeneous bubble growth, stable mass flux without efficient outgassing and continuous magma discharge at the surface. The delicate balance between decompression, volatile exsolution and crystallisation dictates the dynamics of magma ascent, through the buoyancy conferred by the evolving density contrast between magma and crust.

The interplay of the processes described herein leads to varying magma properties and ascent styles across the compositional range of silicate magmas. In basaltic systems, high magmatic temperatures tend to promote lower magma viscosity and relatively high ascent rates, although volatile content is variable (e.g. drier mid-ocean ridge basalts versus wetter arc basalts), leading to variations in crystal content and accompanying variations in latent heat of crystallisation, viscosity and ascent rate. Bubbles can ascend buoyantly and efficiently outgas, decoupled from the magma, or at high ascent rates bubbles and magma may remain coupled, facilitating fragmentation. In intermediate systems (e.g., andesites and dacites), comparatively lower ascent rates promote extensive decompression-induced crystallisation of anhydrous phases such as plagioclase and pyroxene, increasing magma viscosity, which further decreases ascent rate, and encourages open-system degassing (outgassing) and crystallisation. As a result, at shallow levels intermediate magmas are typically very crystal-rich (phenocrysts and extensive microlite formation) with a viscous high-silica melt phase (often rhyolitic). These magmas are among the most viscous on Earth. The high viscosity of rhyolitic magmas typically precludes extensive microlite crystallisation due to low diffusion rates, whilst the relatively high buoyancy promotes higher ascent rates, disequilibrium devolatilisation and high overpressures. In high viscosity systems (intermediate and rhyolitic magmas), bubbles cannot ascend buoyantly and bubble growth is hampered. This can cause overpressure in the coupled magma-gas system, and lead to the brittle fragmentation at the source of explosive eruptions.

Alternatively, permeable outgassing through stalled or slowly-ascending, high viscosity, fractured magma can result in lava effusion.

Despite our extensive knowledge of phase equilibria and volatile solubility, a relatively unconstrained aspect of the evolution of magmas during ascent is temperature. Temperature may change dynamically through the conduit, where the complex and intertwined processes of crystallisation, gas exsolution, gas expansion and outgassing compete, in turn impacting magma viscosity (Fig. 1c). Specifically, bubble growth is endothermic, whereas latent heat of crystallisation can raise the temperature, and the flow of magmatic suspensions can induce shear heating. As such, pressure, temperature and chemical composition evolve dynamically throughout the ascent, and suspension viscosity does not necessarily systematically increase as magma approaches the surface.

Flow dynamics are controlled by all the feedback processes above. Flow in volcanic conduits typically results in lateral variations in ascent rate, causing shear of the magma, with the flow profile dictated by magma viscosity. In Newtonian bodies in which viscosity does not depend on strain rate, strain is pervasive across the width of the conduit and the laminar flow is described by the Hagen–Poiseuille law. In non-Newtonian bodies in which viscosity depends on the rate of deformation, strain localises towards the conduit margins, and is referred to as plug-like flow. In inclined conduits or dykes the situation may be further complicated as the anisotropic distribution of phases may perturb the ascent of magma.

The described wide-ranging variations in magma properties during ascent lead to a spectrum of eruptive behaviour, linked with a variety of volcano morphologies [E6] and hazards (Parts 4, 5 and 6). In basaltic systems, lava fountaining is common, resulting from high ascent rates linked with high magma velocities and significant overpressure. Hazards associated with these eruptions may include spatter-fed lava flows and fine ash due to fragmentation above the vent. High lava fountains are promoted by initially high magma temperatures and lower crystal contents (e.g., hot spot basalts compared to arc basalts). Basaltic sub-Plinian and Plinian eruptions can occur under particular storage and conduit conditions, which cause high decompression rates, high undercooling, and rapid crystallisation, leading to a rapid viscosity increase, extensive brittle fragmentation and much greater hazards such as pyroclastic density currents. In intermediate systems (using a broad classification from basaltic andesites to dacites), high crystal content and high magma viscosity commonly lead to the formation of lava domes and magma plugs with a range of properties, with effusive-explosive transitions likely. Finally, in highly silicic systems, crystal-poor, water-rich rhyolites commonly ascend rapidly from shallow storage, leading to violent explosive eruptions due to high magma velocities and high overpressures in the conduit. This explosive behaviour may transition to the extrusion of late-stage domes composed of viscous, sintered, explosively fragmented pyroclasts.

Evolution during lava emplacement

Once the magma reaches the surface it has two fates: it may either be released explosively via fragmentation or it may emerge as lava, flowing on the surface in effusive eruptions. Lava is a three-phase mixture wherein crystals and bubbles are suspended within a silicate melt phase. In basaltic lavas, the crystals and bubbles typically account for less than 50 vol.% of the mixture. Exceptions include lava with foamy, scoriaceous to pumiceous texture with up to 80 vol.% bubbles, and lava with higher silica content (andesite to rhyolite) that may contain high crystal fractions up to 60 vol.%. When reaching the surface,

the lava cools and devolatilises, triggering crystallisation and interstitial melt differentiation, as well as bubble growth, coalescence and waning (Figs. 1b and 1c). These processes drive continuous evolution of the chemical and physical properties of the lava. Lava texture varies both spatially (from base to surface and from vent to front) and temporally (throughout lava flow emplacement, as cooling and devolatilisation occur). The resultant transformation leads to variations in the rheological properties (viscosity, yield strength, strain rate dependence) of the material being transported, directly influencing the dynamics of flow emplacement. Understanding the thermo-rheological evolution of flowing lava is therefore crucial for modelling and risk management.

The physical properties of lava and their evolution at the surface depend on the lava flow type, which is determined by the appearance of the flow crust. Basaltic lavas typically form pāhoehoe flows, characterised by a smooth surface, and 'ā'a flows characterised by a clinkery fragmented surface, while intermediate (andesite to dacite) and silicic (rhyolite and obsidian) lavas form block flows.

Pāhoehoe flows are composed of low-viscosity lava with a relatively low crystal content and may have a high vesicularity (e.g. s-type pahoehoe). 'Ā'a flows have a higher viscosity. They are composed of an advancing dense and molten lava core surrounded by fragmented surface and base layers, composed of scoriaceous, high porosity, irregular fragments. These flows may develop a channel where the lava moves efficiently between stable levees. In sheared zones, such as on the edge of the channel, crystals may align, and bubbles may deform, both reducing viscosity and facilitating its flow, while bubbles may wane due to outgassing, increasing the lava viscosity. Mafic lavas erupt at temperatures up to 1200°C, and exhibit relatively low viscosity ($<10^3$ Pa·s). Their low viscosity and high element diffusivity enable crystallisation and devolatilisation, resulting in a significant viscosity increase of several orders of magnitude from the vent to the front. Referred to as cooling-limited conditions or rheological cut-off, the lava stops flowing when reaching the upper limit of apparent flow viscosity around 10^4–10^6 Pa·s. However, this rheological cut-off depends not only on the final thermo-rheological conditions but also on crystallisation and cooling history, pre- and syn-eruption kinetics and strain rate. Basaltic lava flows may also undergo a transition from pāhoehoe to 'ā'a, characterised by a change in rheological flow behaviour as the more viscous lava becomes more susceptible to shear stress that can tear it apart and form fragments. This transition is dependent on the increase of both viscosity during cooling and shear rate with increasing flow velocity, due to steep slopes or high effusion rates.

Intermediate and silicic lavas are the most viscous and the thickest lava flows, reaching thicknesses of up to hundreds of metres, and move slowly. These lavas may have a high crystallinity and typically have a low porosity, as is the case for most intermediate lavas, e.g., andesitic or dacitic lava, but they may also appear glassy, near aphyric, and possess highly vesicular layers, as in obsidian flows. Intermediate to silicic lavas erupt at temperatures around 900 to 1100°C, resulting in typical viscosities between 10^5 to 10^9 Pa·s, and maximum viscosities around to 10^{12}–10^{13} Pa·s, forming lava domes and spines. During flow and cooling, crystallisation is hindered by the high viscosity and consequent low element diffusion rates, and hence does not significantly affect the flow. The lava is usually already degassed with no clear evidence of downflow variation, but there is evidence of outgassing via surface vesiculation forming a scoriaceous carapace. The halt of such thick flows is dominantly due to the increasing thickness and yield strength of the growing carapace. Two theories exist regarding blocky lava flows: they advance either like a caterpillar (similar to 'ā'a flows), where the core is composed of molten material moving as a viscous flow capable of folding; or like a glacier, where the flow slides on a shear zone over a brecciated surface, forming fracture-bound ogives.

During emplacement, as cooling proceeds and phase proportions change, lava density may change too. When outgassing occurs, up to 50 vol.% of the bubbles can be removed, and the lava's density can double. However, this increase in density has a smaller impact on lava mobility compared to changes in viscosity.

The cooling of lava flows during emplacement happens mainly through radiation from the hot flow surface into the atmosphere. The surface temperature of lava decreases significantly (to the power of four; Eq. 2) and rapidly (over seconds) upon eruption, forming a cooler crust or rind. Another heat loss mechanism is linked to the temperature difference between the lava surface and the air, generating air convection, where the heat from the lava surface is carried away by the cooler air (that may be forced due to wind), lowering the surface temperature (Eq. 5). A third cooling mechanism is by heat conduction from the lava into the ground and levees, but this is a slow process due to lavas' poor conductivity. Additional lava flow cooling is due to cooler material entrainment and environmental conditions such as rain. Overall, open-channel lava flows lose heat rapidly, while well-insulated lava, such as in lava tubes, may conserve its heat and travel long distances. The estimated heat loss during basaltic lava flow emplacement is around a few degrees per km, while lava in tubes cools more slowly. Heat is also produced in lava flows as a result of latent heat of crystallisation and viscous heating due to motion (becoming important on slopes of a few degrees or more). However, this heat production is significantly overshadowed by the heat loss, inevitably leading to the flow cooling. Lava flow thermo-rheological properties can be calculated along a lava flow using the combined model FLOWGO [13], which calculates the heat budget within a control volume of lava as lava moves within a channel away from the vent at a constant effusion rate. This 1D model allows the retrieval of viscosity changes due to heat loss, and hence lava velocity until it reaches zero, defining the flow runout distance.

Lava viscosity during emplacement can be estimated using a combination of models that consider the chemical composition and temperature of the melt phase, as well as crystal and bubble fractions and aspect ratios (as discussed in the section above). Laboratory measurements on remelted rock samples can also be conducted to obtain the viscosity-temperature relationship of the lava across super- and sub-liquidus conditions. Such experiments may be conducted at thermodynamic equilibrium or disequilibrium, under constant cooling, which may help to define the rheological cut-off. Nevertheless, laboratory measurements struggle to reproduce exact field conditions (crystal and bubble nature, proportion, redox states) during lava emplacement. Measuring the viscosity of lava in-situ has the potential to bridge the gap between field conditions and laboratory constraints. This approach is restricted to basaltic lavas (block lavas being too hazardous to approach), and the rapid cooling of the lava surface is a limitation. Only a few studies have attempted such challenging measurements, but recent developments are promising for the near future.

Summary

In this chapter, the physical and thermodynamic properties of magma are reviewed in the context of magma storage, transport, eruption and emplacement. A theoretical framework to model volcanic eruptions has been developed and begun to be used for the prediction of volcanic activity [E7] – a deep understanding of magma's physical properties is fundamental to making progress in those studies. Whilst heat flow processes and the thermal properties of magmas are well understood, and theoretical relationships to calculate magma permeability and two-phase magma rheology are available, magma

properties and reaction kinetics under dynamic conditions remain poorly constrained. For instance, empirical models have been developed to predict the viscosity and brittle failure of silicate melt; however, the understanding of molecular scale changes in silicate melt and magma under deformation is still lacking. The understanding of multiphase magma rheology also remains a key area of research, in particular the complex interactions between crystals, bubbles and melt over the wide range of conditions characterising magmatic-volcanic systems. The proactive utilisation of new experimental and computational technologies is essential for advancing our understanding of magma's physical properties and their influence on volcanic eruption styles and hazards.

References

[1] J.E. Stebbins, I.S.E. Carmichael, L.K. Moret, Heat capacities and entropies of silicate liquids and glasses. Contri. Mineral. Petrol. 86 (1984) 131–148, https://doi.org/10.1007/BF00381840.

[2] Y. Fei, Thermal expansion, in: T.J. Ahrens (Eds), Mineral physics and crystallography, A handbook of physical constants. American Geophysical Union, Washington DC (1995) 29–44.

[3] A.M. Hofmeister, A. Sehlke, G. Avard, A.J. Bollasina, G. Robert, A.G. Whittington, Transport properties of glassy and molten lavas as a function of temperature and composition. J. Volcanol. Geotherm. Res. 327 (2016) 330–348, https://doi.org/10.1016/j.jvolgeores.2016.08.015.

[4] D. Giordano, J.K., Russell, D.B. Dingwell, Viscosity of magmatic liquids: a model. Earth Planet. Sci. Lett. 271(2008), 123–134.

[5] H.M. Mader, E.W. Llewellin, S.P. Müller, The rheology of two-phase magmas: a review and analysis. J. Volcanol. Geotherm. Res. 257 (2013) 135–158, https://doi.org/10.1016/j.jvolgeores.2013.02.014.

[6] A. Costa, Viscosity of high crystal content melts: Dependence on solid fraction. Geophys. Res. Lett., 32 (2005) L22308, https://doi.org/10.1029/2005GL024303.

[7] S.H. Maron, P.E. Pierce, Application of ree-eyring generalized flow theory to suspensions of spherical particles. J. Colloid Sci. 11 (1956) 80–95, https://doi.org/10.1016/0095-8522(56)90023-X.

[8] A. Frontoni, A. Costa, A. Vona, C. Romano, A comprehensive database of crystal-bearing magmas for the calibration of a rheological model. Sci. Data 9 (2022) 247, https://doi.org/10.1038/s41597-022-01363-w.

[9] E.W. Llewellin, H.M. Mader, S.D.R. Wilson, The rheology of a bubbly liquid. Proc. R. Soc. Lond. A 458 (2002) 987–1016, https://doi.org/10.1098/rspa.2001.0924.

[10] M. Pistone, B. Cordonnier, P. Ulmer, L. Caricchi, Rheological flow laws for multiphase magmas: An empirical approach. J. Volcanol. Geotherm. Res. 321 (2016) 158–170, https://doi.org/10.1016/j.jvolgeores.2016.04.029.

[11] N. Phan-Thien, D.C. Pham, Differential multiphase models for polydispersed suspensions and particulate solids. J. Non-Newtonian Fluid Mech. 72 (1997) 305–318, https://doi.org/10.1016/S0377-0257(97)90002-1.

[12] G. Ranalli, Rheology of the Earth (second ed.), Chapman and Hall, London (1995) pp. 413.

[13] A.J. Harris, S. Rowland, FLOWGO: a kinematic thermo-rheological model for lava flowing in a channel, Bull. Volcanol. 63 (2001) 20–44, https://doi.org/10.1007/s004450000120.

[14] B.A. Halverson, A. Emerson, J. Hammer, J. Lira, A. Whittington, Estimates of crystallinity utilizing Differential Scanning Calorimetry: Application to the Kilauea 2018 Lower East Rift Zone eruption. J. Petrol. 65 (2024) egae010, https://doi.org/10.1093/petrology/egae010.

[15] A.G. Whittington, A.M. Hofmeister, P. Nabelek, Temperature-dependent thermal diffusivity of Earth's crust and implications for magmatism. Nature 458 (2009) 319-321, https://doi.org/10.1038/nature07818.

[16] J.D. Merriman, A.G. Whittington, A.M. Hofmeister, P.I. Nabelek, K. Benn, Thermal transport properties of major Archean rock types to high temperature and implications for cratonic geotherms. Precam. Res. 233 (2013) 358–372, https://doi.org/10.1016/j.precamres.2013.05.009.

[17] J. Blower, Factors controlling permeability–porosity relationships in magma. Bull. Volcanol. 63 (2001) 497–504, https://doi.org/10.1007/s004450100172.

[18] S. Mueller, O. Melnik, O. Spieler, B. Scheu, D.B. Dingwell, Permeability and degassing of dome lavas undergoing rapid decompression: an experimental determination. Bull. Volcanol. 67 (2005) 526–538, https://doi.org/10.1007/s00445-004-0392-4.

[19] R.W. Zimmerman, G.S. Bodvarsson, Hydraulic conductivity of rock fractures. Transport in porous media 23 (1996) 1–30.

[20] F.B. Wadsworth, J. Vasseur, E.W. Llewellin, R.J. Brown, H. Tuffen, J.E. Gardner, J.E. Kendrick, Y. Lavallée, K.J. Dobson, M.J. Heap, D.B. Dingwell, A model for permeability evolution during volcanic welding. J. Volcanol. Geotherm. Res. 409 (2021) 107118, https://doi.org/10.1016/j.jvolgeores.2020.107118.

References in the 2nd and 3rd editions of EoVs

[E1] L. France, E. Green, P.L. Marquez, J. Blundy, B Carvalho, B. Charlier, S. Lambart, M. Pistone, T. Shea, M. Holness, The origin and composition of magmas, in: C. Bonadonna, L. Caricchi, A. Clarke, P. Cole, J. Lindsay, J. Lowenstern, R. Robertson, M. Villegas (Eds.), Encyclopedia of Volcanoes (third edition), Elsevier (2026), Part 1, Chapter 2.1.

[E2] A. Schmidt, Y. Zhu, P. Yu, M. Sigl, P. Sellitto, P. Huybers, T. Aubry, J.I. Farquharson, M. Hartley, T. Thordarson, B. Black, Impact on climate, in: C. Bonadonna, L. Caricchi, A. Clarke, P. Cole, J. Lindsay, J. Lowenstern, R. Robertson, M. Villegas (Eds.), Encyclopedia of Volcanoes (third edition), Elsevier (2026), Part 4, Chapter 2.7.

[E3] M. Edmonds, T. Fischer, A. Shahar, K. Iacovino, A.-S. Bouvier, K. Roggensack, D. Sellés, P. Caffe, S. Guzmán, E. Hughes, Origins of magmatic volatiles and their role in magma ascent and degassing, in: C. Bonadonna, L. Caricchi, A. Clarke, P. Cole, J. Lindsay, J. Lowenstern, R. Robertson, M. Villegas (Eds.), Encyclopedia of Volcanoes (third edition), Elsevier (2026), Part 1, Chapter 2.2.

[E4] C.E. Lesher, F.J. Spera, Thermodynamic and Transport Properties of Silicate Melts and Magma, in: H. Sigurdsson, B.F. Houghton, S.R. McNutt, H. Rymer, J. Stix (Eds.), Encyclopedia of Volcanoes (second edition), Elsevier (2015), 113–141.

[E5] E. Rivalta, L. Passarelli, J. Kavanagh, M. Coombs, J. Hammer, C. Martel, G. Kilgour, Y. Aoki, M. Nikkhoo, C. Meriaux, Magma Ascent, in: C. Bonadonna, L. Caricchi, A. Clarke, P. Cole, J. Lindsay, J. Lowenstern, R. Robertson, M. Villegas (Eds.), Encyclopedia of Volcanoes (third edition), Elsevier (2026), Part 1, Chapter 5.2.

[E6] A. Graettinger, A. Diefenbach, M. Ort, K. Bemis, E. Paguican, P. Grosse, Volcano types and their morphology, in: C. Bonadonna, L. Caricchi, A. Clarke, P. Cole, J. Lindsay, J. Lowenstern, R. Robertson, M. Villegas (Eds.), Encyclopedia of Volcanoes (third edition), Elsevier (2026), Part 2, Chapter 3.1.

[E7] B. Kaus, C. Michaut, C. Annen, M. Townsend, O. Melnik, T. Keller, G. Bergantz, O. Galland, R. Nicolas. Modelling of magma storage and transport, in: C. Bonadonna, L. Caricchi, A. Clarke, P. Cole, J. Lindsay, J. Lowenstern, R. Robertson, M. Villegas (Eds.), Encyclopedia of Volcanoes (third edition), Elsevier (2026), Part 1, Chapter 5.3.

"Case-study box"

The viscosity of a dacitic melt that corresponds to the bulk rock composition of erupted products from the 18 May 1980 Plinian activity of Mount St Helens is calculated to be 4.0×10^3 Pa·s, using a well-established melt viscosity model [4] and assuming a temperature of 875°C and a water content of 4.6 wt.%. However, the groundmass composition of erupted products is rhyolitic, and for this composition melt viscosity is calculated to be 2.2×10^4 Pa·s. The viscosity of the crystal-bearing magma (i.e., the suspension viscosity) with a rhyolitic melt must therefore be calculated, obtaining 1.7×10^5 Pa·s from Eq. 8, considering a crystal content of 35 vol.%. This viscosity corresponds to that estimated in the reservoir, and will change during ascent and emplacement due to devolatilisation and bubble formation (Fig. 1c). Ascent to shallow parts of the conduit results in decompression, devolatilisation and bubble formation. The viscosity of the rhyolitic melt when it reaches the point of fragmentation at 8 MPa is 2.8×10^7 Pa·s, at which point the water concentration is 0.56 wt.% H_2O. Here, the suspension viscosity is calculated to be 2.2×10^8 Pa·s from Eq. 8 with a crystal content of 35 vol.%. Eq. 14 can be applied to calculate the viscosity of the bubble-bearing suspension. When Ca >>1, that is, the magma ascends rapidly and is highly vesiculated (gas volume of 80 vol.%), resulting in fragmentation and an explosive eruption, the viscosity is 1.5×10^7 Pa·s. In this example, the viscosity of the magma increased by almost two orders of magnitude between the reservoir and the shallow conduit. In the supplementary exercises, the calculation process is explained in detail and a ternary diagram between pure melt, solid (crystals) and gas bubbles is used to track magma evolution according to different ascent paths.